Electronic Supplementary Information

Single-center Ln^{III} ratiometric luminescent temperature probe based on singlet → singlet and singlet →triplet sensitizations

Airton Germano Bispo-Jr,[a] Italo Odone Mazali,[a] Fernando Aparecido Sigoli[a]*

[a.] Department of inorganic chemistry, Institute of Chemistry, University of Campinas, Unicamp, Josué de Castro street, Cidade Universitária, Campinas, 13083-970

Table of Contents

Supplementary note S1 – Synthesis and characterization

Chemicals

Si-H terminated poly(dimethylsiloxane) (PDMS, Aldrich), toluene (Merck, 99%), allyldiphenylphosphine oxide (adppo, Aldrich, 96%), tetravinylsilane (ABCR), and divinyltetramethyldisiloxanoplatin(0) were used as starting reactants. All powder precursor complexes were synthesized by employing a methodology previously reported by us.[1]

Membrane synthesis

First, Si-H terminated PDMS was functionalized with adppo to enable its coordination to the Ln^{III} center following a procedure optimized by Gaspar and coworkers.[2] For that, PDMS (2.0 mg) was added in a round-bottom flask (upon N_2 atmosphere) with 5 mL of dried toluene, followed by the addition of adppo (17.0 mg, 1 mol% in relation to the number of Si-H bonds). After that, 1 drop of the divinyltetramethyldisiloxanoplatin(0) catalyst (Karsted catalyst) was added and the reaction was kept upon stirring at 25 ºC for 2 hours to enable the bond of adppo to PDMS, changing adppo to propyldiphenylphosphine oxide (pdppo). In the second step, the complex was mixed with the previously functionalized PDMS polymer in toluene. For that, 0.036 mmol of complex (mol proportion of 1:2 of complex:adppo) was added in the previous mixture and the solution was kept under stirring for 2 hours at 25 ºC upon N_2 atmosphere. After that, for PDMS reticulation, tetravinylsilane (0.222 mL, referent to the other 99% of Si-H bonds) was added followed by two drops of the divinyltetramethyldisiloxanoplatin(0) catalyst. Finally, the solution was transferred to a circular Teflon support (4 cm of diameter) which was dried at 40 ºC for 24 hours. Figure S1 brings a scheme of the reactional steps regarding the syntheses of PDMS membranes with pictures of membranes upon white light and UV radiation exposition.

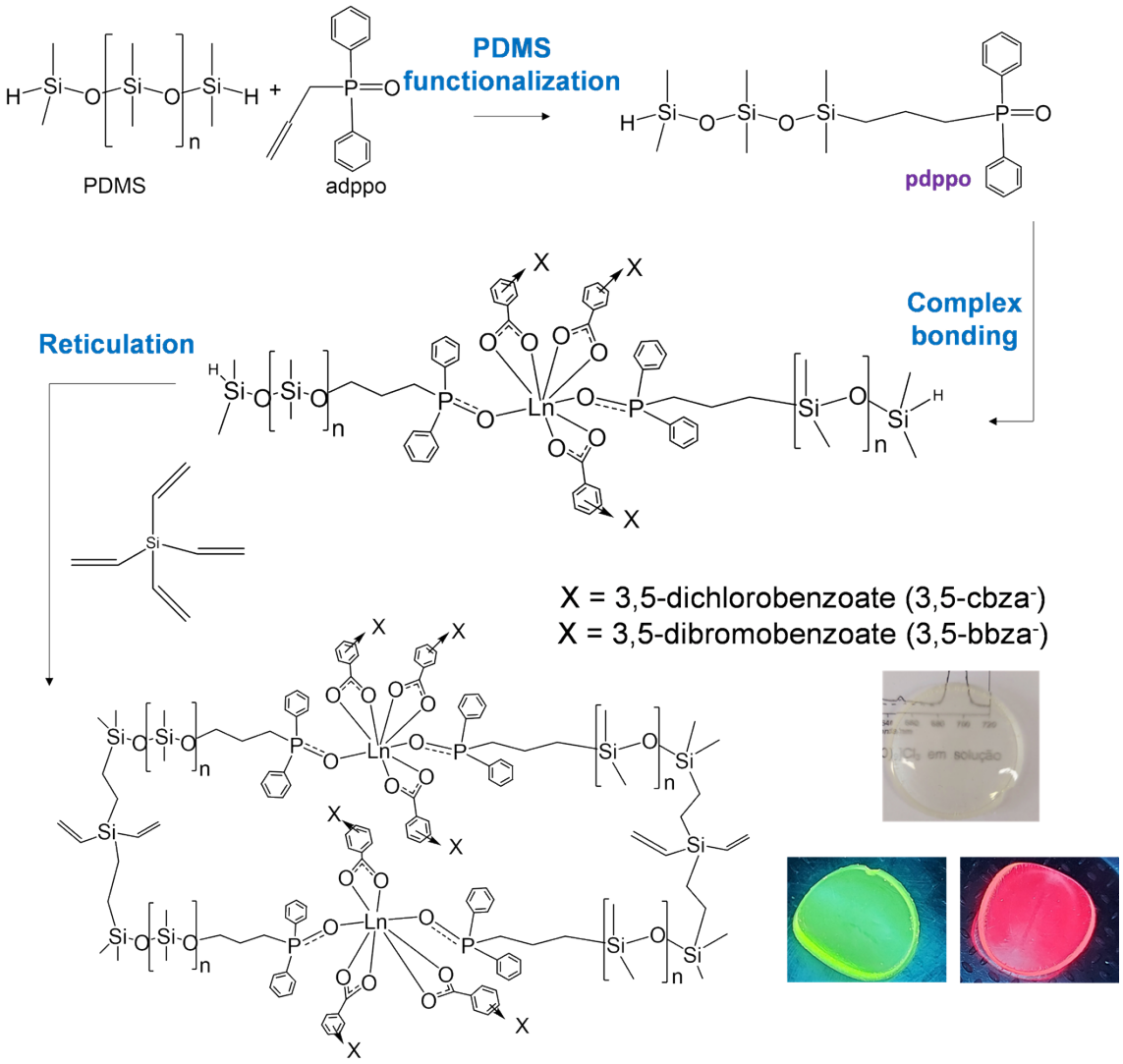

Figure S1. Reaction scheme representing the PDMS functionalization with adppo, complex bonding, and reticulation with tetravinylsilane. Insert represents the pictures of PDMS membranes upon white light and UV (254 nm) exposition: [Tb(3,5-cbza)$_3$(pdppo)$_2$]-PDMS (left) and [Eu(3,5-cbza)$_3$(pdppo)$_2$]-PDMS (right).

Characterization

FTIR: FTIR of membranes were measured in a FTIR Agilent Cary 630 spectrophotometer in the attenuated total reflectance (ATR) mode with increment of 2 cm^{-1}.

Diffuse reflectance spectroscopy (DRS)**.** DRS (increment of 1 nm) were obtained in the absorbance mode by employing a SHIMADZU UV-2450 spectrometer and $BaSO_4$ as reflectance standard.

Steady-state photoluminescence: Photoluminescence excitation and emission spectra (298 K, excitation and emission slits close to 0.5 mm) of Eu^{III} and Tb^{III} membranes were carried out in a Horiba Jobin-Yvon FL3-22-iHR-320 equipment (front face mode) by using as excitation source a Xe (450 W) lamp.

All spectra were corrected accordingly to the photodetector (Hamamatsu PMT) and Xe lamp intensity. For Yb^{III} membranes, emission spectra were measured in a Sdrive-500 Horiba CCD camera and the excitation spectra were carried out by using a Hamamatsu H10330-75 detector.

Time-resolved spectroscopy: Time-resolved spectroscopy was obtained by using a 150 W xenon lamp and a Time-Correlated Single Photon Count (TCSPC) system equipped in the Horiba FL3-22-iHR320 spectrofluorometer at 298 K. Emission decay curves were measured in triplicate and fitted through a monoexponential adjustment.

Epifluorescence. Epifluorescence imagens in the dark field mode were acquired in Leica DM IRB epifluorescence microscope.

Temperature-dependent excitation and emission spectroscopy: Excitation and emission spectra from 30 K to 325 K were measured in the previously mentioned Fluorolog 3 equipment. To control the temperature, a Janis cryostat (CCS-100/204N model) with an Acme Electric compressor (T181059 model) and a Lake Shore temperature controller (model 335) were used. The relative thermal sensitivity is calculated from Equation S1, where *Δ* is the thermometric parameter and *T* is the temperature. The temperature uncertainty (*δT*) is calculated by Equation S2, where *δI/I* is the relative uncertainty in the integrated area.

$$S_r = \frac{1}{\Delta}\left|\frac{d\Delta}{dT}\right| (S1) \qquad \delta T = \frac{1}{S_r}\frac{\delta\Delta}{\Delta} (S2) \qquad \frac{\delta\Delta}{\Delta} = \sqrt{\left(\frac{\delta I_1}{I_1}\right)^2 + \left(\frac{\delta I_2}{I_2}\right)^2} (S3)$$

Absolute emission quantum yield. Emission quantum yield (Φ_L^{Ln}) was measured in a Quanta -φ F-3029 integrating sphere coupled by optic fibers to the previously mentioned Fluorolog 3. The empty sphere coated with Spectralon® (reflectance > 95%) was used as absorption reference. Equation S4 was used for the calculation, where N_{Em} and N_{Abs} are the number of photons emitted and absorbed by the sample, respectively, I_{em} is the emission spectrum of the sample, and I_{ex} and I_{ex}^{st} stand for the excitation spectra of the light used to excite the sample and the integrating sphere empty, respectively.

$$\Phi_L^{Ln} = \frac{N_{Emi}}{N_{Abs}} = \frac{\int_{\lambda_1}^{\lambda_2} I_{em}(\lambda)d\lambda}{\int_{\lambda_3}^{\lambda_4} I_{ex}^{st}(\lambda)d\lambda - \int_{\lambda_3}^{\lambda_4} I_{ex}(\lambda)d\lambda} \quad (S4)$$

Supplementary note S2 – Structure of PDMS membranes

FTIR spectra of PDMS membranes, Figure S2, show bands at about 789–796 cm^{-1} assigned to the $-CH_3$ rocking and the Si-C stretching in $Si-CH_3$ group, 1020–1074 cm^{-1} ascribed to Si-O-Si stretching, 1260–1259 cm^{-1} due to CH_3 deformation in $Si-CH_3$, and 2950–2960 cm^{-1} attributed to the asymmetric CH_3 stretching in $Si-CH_3$.[3] These vibrational modes agree with those reported for other PDMS membranes,[3] confirming the successful structure formation. Vibrational modes characteristic of complexes are not noticed in the FTIR spectra due to the low weight fraction compared with the polymeric matrix, yet, the complex incorporation is confirmed by epifluorescence images of PDMS membranes, Figure S3, which revel fine complex dispersion lacking particle agglomerates in the measured spatial range of 100 µm (20x magnification).

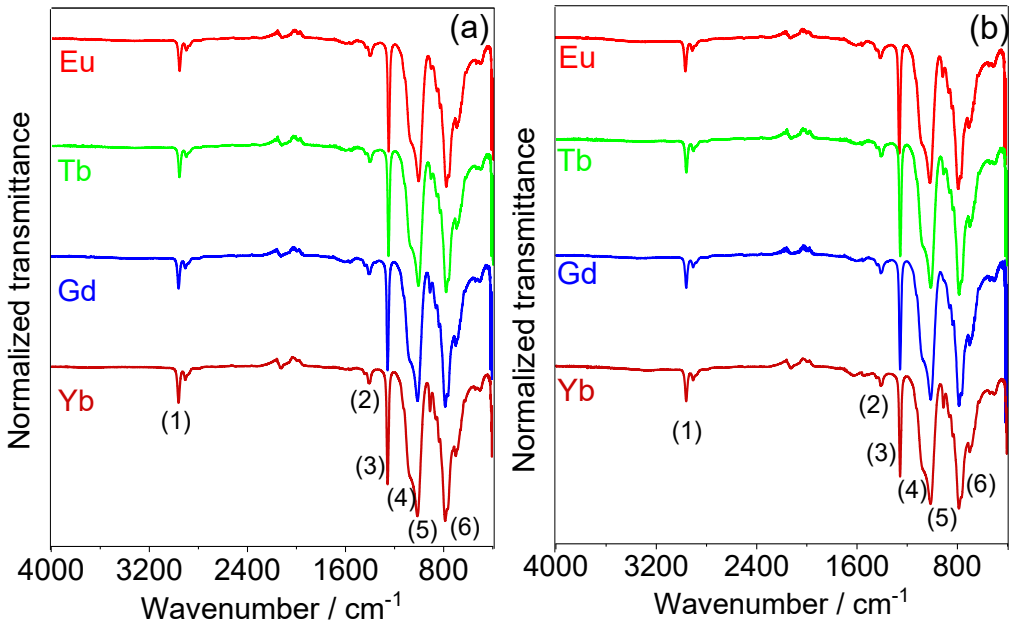

Figure S2. FTIR spectra of (a) $[Ln(3,5\text{-cbza})_3(pdppo)]$-PDMS and (b) $[Ln(3,5\text{-bbza})_3(pdppo)]$-PDMS (Ln = Eu^{III}, Tb^{III}, Gd^{III}, and Yb^{IIII}). Assignments: (1) asymmetric CH_3 stretching in $Si-CH_3$, (2) symmetric C=C stretching, (3) CH_3 deformation in $Si-CH_3$, (4) asymmetric Si-O-Si stretching, (5) symmetric Si-O-Si stretching, and (6) $-CH_3$ rocking and Si-C stretching in $Si-CH_3$.

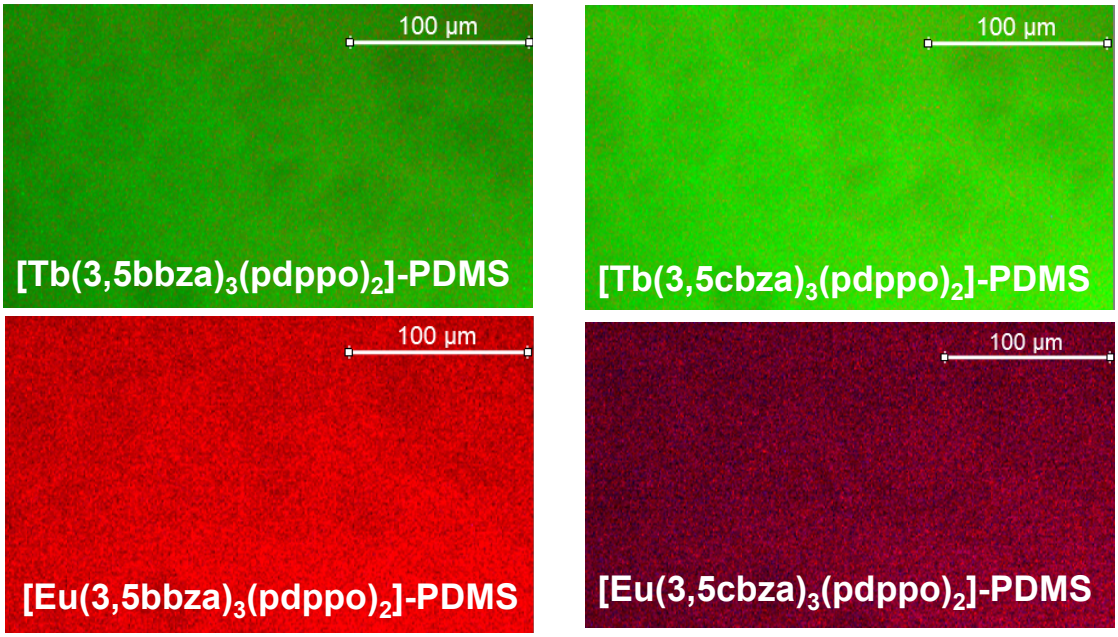

Figure S3. Epifluorescence images (dark field) with 20x magnification of Tb^{III} or Eu^{III} complexes in the PDMS membrane (λ_{exc} = 375 m).

Supplementary note S3 – DRS spectra and triplet state energy and Gd^{III} complexes

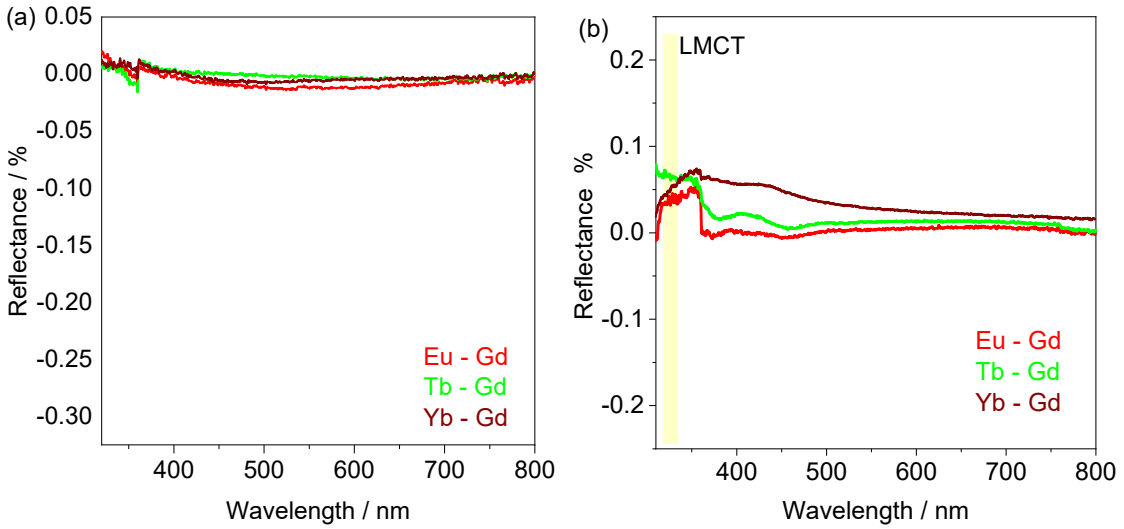

Figure S4. Arithmetic difference between the DRS spectra of Ln^{III} (Eu, Tb, or Yb) systems and analogous Gd^{III} one for the (a) [Ln(3,5-cbza)$_3$(pdppo)]-PDMS or (b) [Ln(3,5-bbza)$_3$(pdppo)]-PDMS series. For the [Ln(3,5-bbza)$_3$(pdppo)]-PDMS series, some bands at 360 nm and 430 nm are observed since the $S_0 \rightarrow T_n$ transition relaxation depends on the spin-orbital coupling effect, which is different depending on the Ln^{III}.

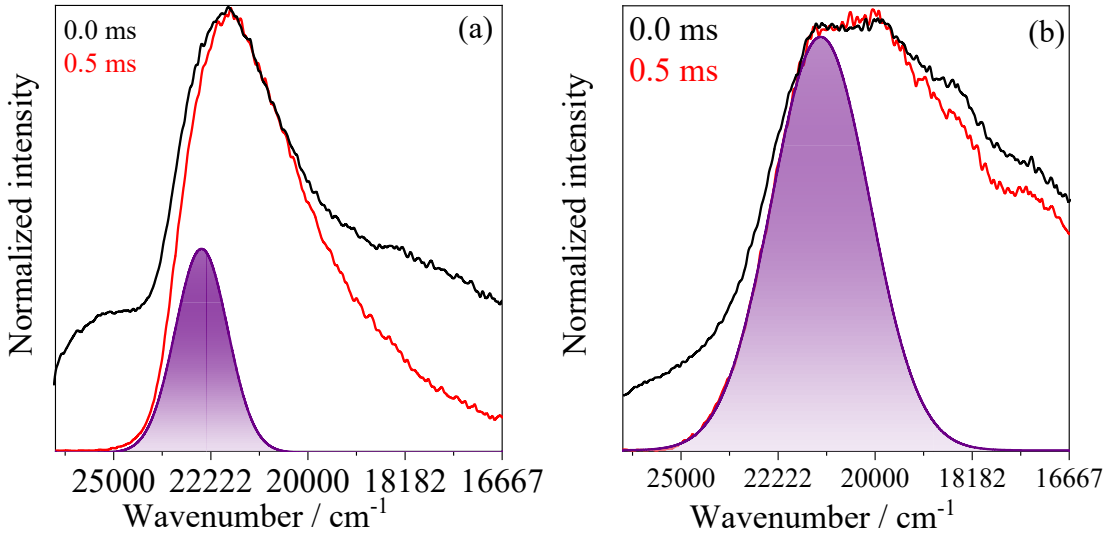

Figure S5. Time-resolved (delay of 0.5 ms) emission spectra (77 K) of Gd^{III} powder complexes compared with the steady-state emission. (a) [Gd(3,5-cbza)$_3$(pdppo)$_2$]-PDMS and (b) [Gd(3,5-bbza)$_3$(pdppo)$_2$]-PDMS. The deconvolution of each spectrum was carried out by applying a gaussian function. To shut off any emission coming from short-lived singlet states or vibronic components, time-resolved emission spectra (77 K) were measured, and the zero-phonon transition was considered to determine the triplet (T_1) state energy through the band energy maximum of the zero-phonon transition.

Supplementary note S4 – Steady-state luminescence

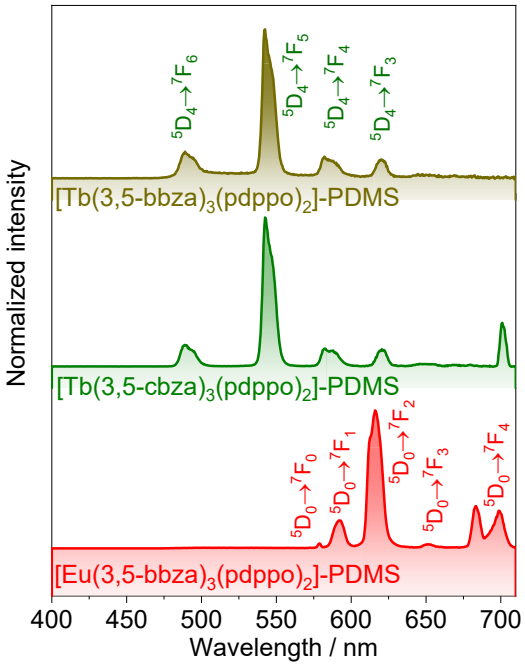

Figure S6. Emission spectra (λ_{exc} = 360 nm) of [Eu(3,5-bbza)$_3$(pdppo)$_2$]-PDMS, [Tb(3,5-cbza)$_3$(pdppo)$_2$]-PDMS, and [Tb(3,5-bbza)$_3$(pdppo)$_2$]-PDMS membranes.

Supplementary note S5 – Time-resolved luminescence and photophysical parameters

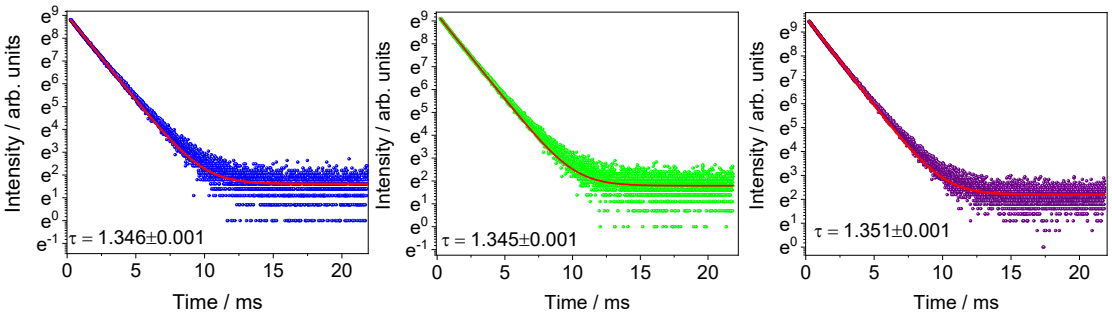

Figure S7. Example of emission intensity decay curves measured in triplicate for the [Eu(3,5-cbza)$_3$(pdppo)$_2$]-PDMS membrane monitored at 293 K. (λ_{exc} = 300 nm, λ_{em} = 612 nm). Curves were fitted through a monoexponential adjustment (R^2 > 0.95).

Table S1. $^5D_0$ state lifetime (τ, ms), radiative (A_{rad}, s^{-1}) and non-radiative (A_{nrad}, s^{-1}) decay probabilities, intrinsic emission quantum yield (Φ_{Ln}^{Ln}, %), and overall emission quantum yield (Φ_{L}^{Ln}, %, error of 10% of the value) of Eu^{III} complexes in PMDS compared with the free-standing complexes. For Tb and Yb complexes, the emitting state lifetime is also represented.

Complexes	λ_{exc}	τ (ms)	A_{rad}	A_{nrad}	Q_{Ln}^{Ln}	Q_{L}^{Ln}
[Eu(3,5-cbza)$_3$(pdppo)$_2$]	300	1.3484±0.0004	465	276	62	-
[Eu(3,5-bbza)$_3$(pdppo)$_2$]	300 360	1.4399±0.0009 1.298±0.001	455 448	239 322	65 58	- < 1
[Tb(3,5-cbza)$_3$(pdppo)$_2$]	300 360	1.828±0.001 1.684±0.001	-	-	-	- 8.9
[Tb(3,5-bbza)$_3$(pdppo)$_2$]	300 360	1.632±0.002 1.283±0.002	-	-	-	- 14

For Eu^{III} membranes, the intrinsic emission quantum yields (Φ_{Eu}^{Eu}) were calculated from Equation S5 by considering radiative (A_{rad}, Equation S6) and non-radiative (A_{nrad}) decay probabilities, and the emitting state lifetime (τ), where $A_{0\lambda}$ is the spontaneous emission probability of a transition, A_{01}=14,6·n^3, n is the refractive index (1.500), S_{0J} is the area under the band assigned to the $^5D_0 \rightarrow {}^7F_J$ transition, and ν_{0J} is the transition energy barycenter.

$$\Phi_{Eu}^{Eu} = \frac{A_{rad}}{A_{Total}} = \frac{\tau_{total}}{\tau_{rad}} \quad (S5)$$

$$A_{0J} = A_{01}\left(\frac{\nu_{01}}{\nu_{0J}}\right)\left(\frac{S_{0J}}{S_{01}}\right) \quad (S6)$$

Supplementary note S6 – Temperature-dependent emission spectra

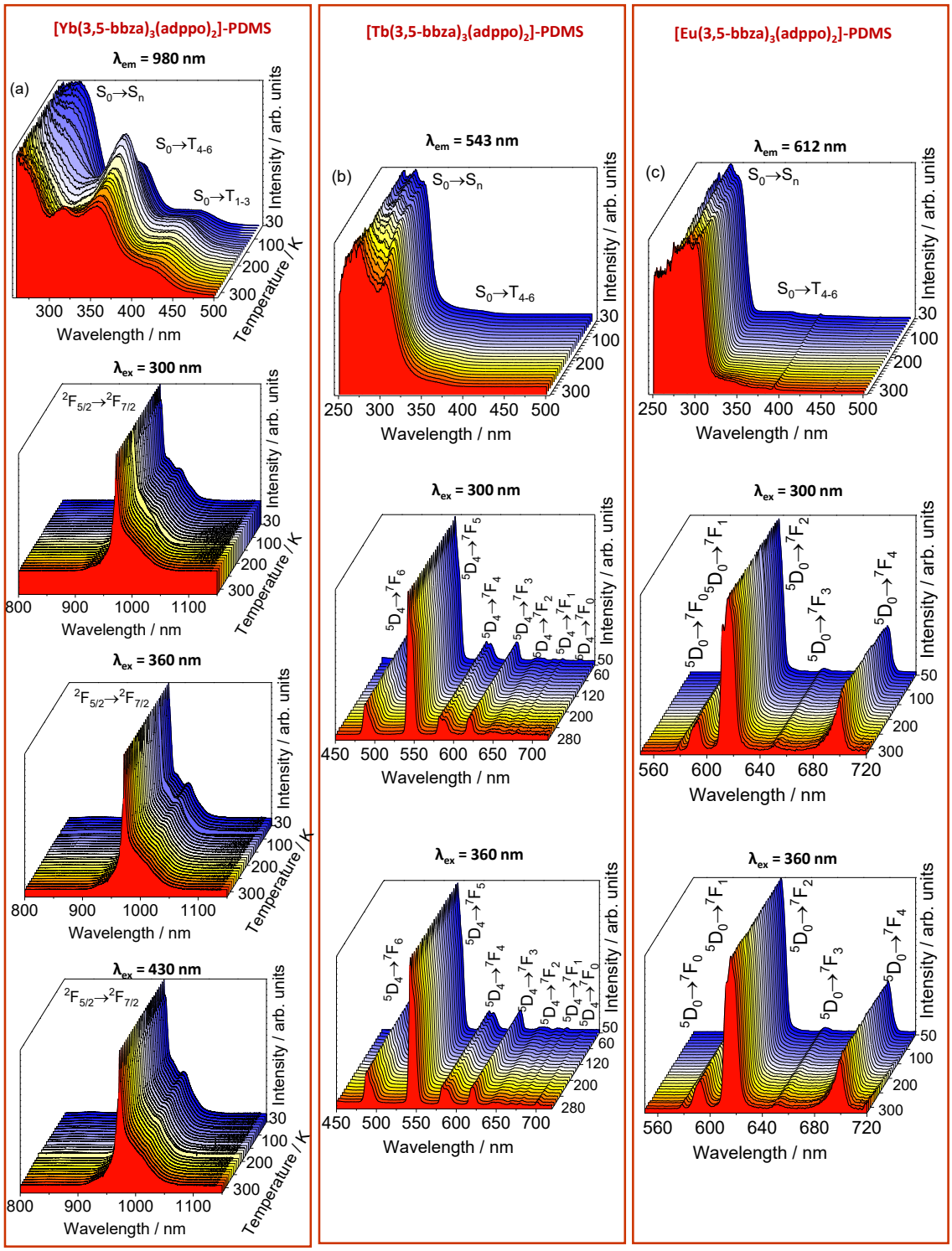

Figure S8. Normalized temperature-dependent excitation and emission spectra of (a) [Yb(3,5-bbza)$_3$(pdppo)$_2$]-PDMS (λ_{em} = 612 nm), (b) [Tb(3,5-bbza)$_3$(pdppo)$_2$]-PDMS (λ_{em} = 543 nm), and (c) [Eu(3,5-bbza)$_3$(pdppo)$_2$]-PDMS (λ_{em} = 980 nm).

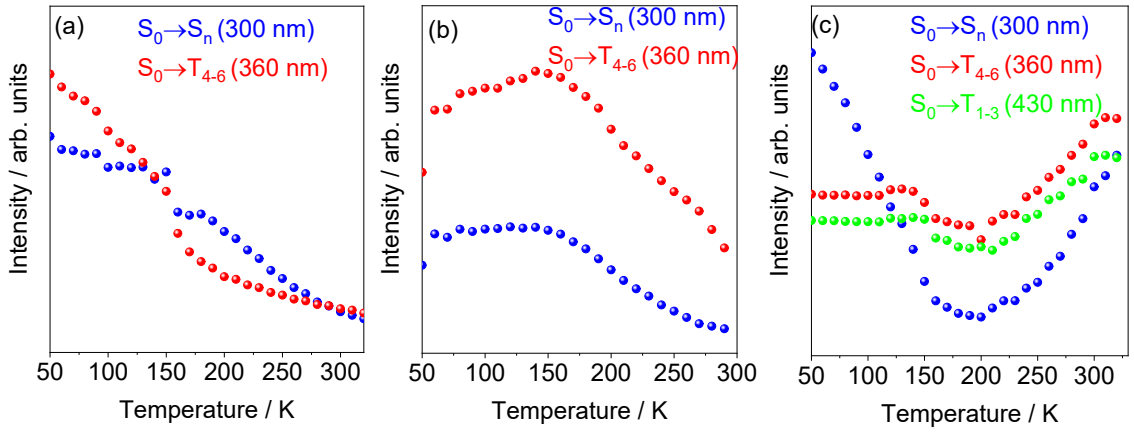

Figure S9. Dependence of the excitation band intensity on temperature for the (a) [Eu(3,5-bbza)$_3$(pdppo)$_2$]-PDMS (λ_{em}= 612 nm), (b) [Tb(3,5-bbza)$_3$(pdppo)$_2$]-PDMS (λ_{em}= 543 nm), and (c) [Yb(3,5-bbza)$_3$(pdppo)$_2$]-PDMS (λ_{em}= 980 nm) membranes.

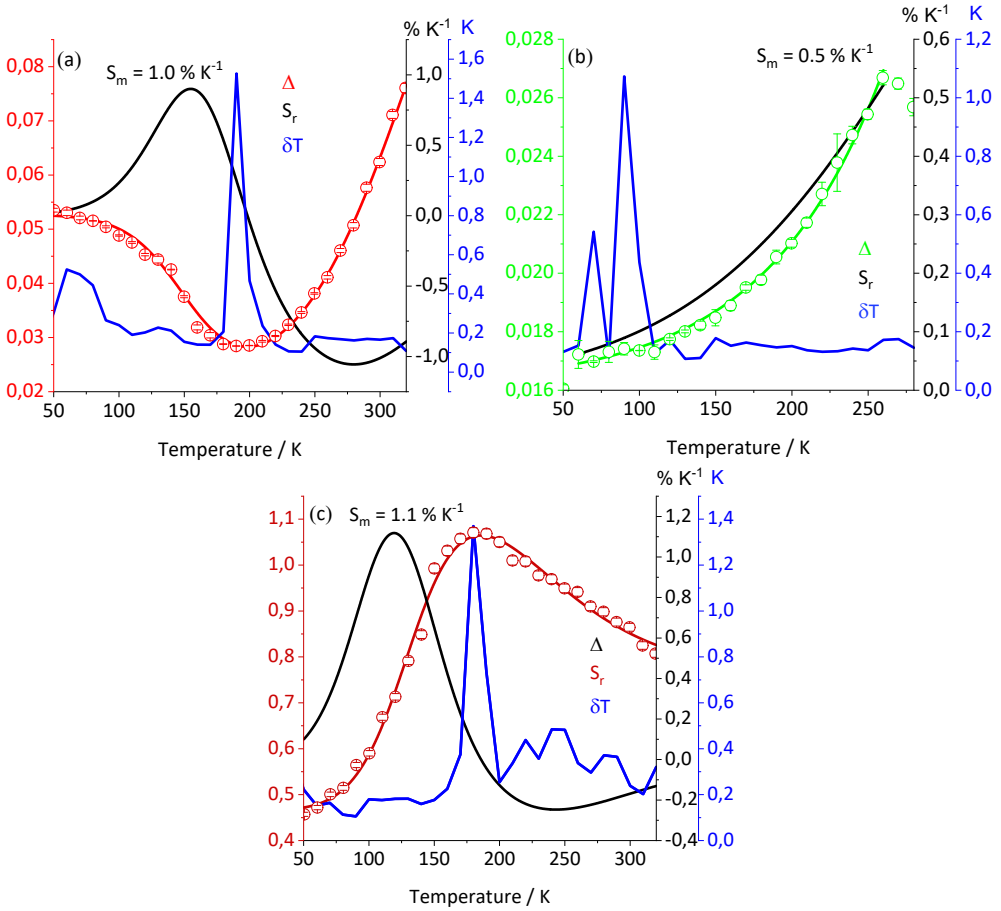

Figure S10. Temperature dependence of thermometric parameter, (Δ) relative thermal sensitivity (S_r), and temperature uncertainty (δT) by considering the area of the excitation bands (excitation intensity ratio method) in (a) [Eu(3,5-bbza)$_3$(pdppo)$_2$]-PDMS, (b) [Tb(3,5-bbza)$_3$(pdppo)$_2$]-PDMS, and (c) [Yb(3,5-bbza)$_3$(pdppo)$_2$]-PDMS

Table S2. Maximum thermal sensitivity (S_m) used as figure of merit within the state-of-the-art of Ln^{III}-based (Ln = Eu, Tb, and/or Yb) systems used as ratiometric luminescent thermometers.

System	Ln^{III}	Method	ΔT / K	S_m / % K^{-1}	T_m / K	ref
$[Eu(3,5\text{-}bbza)_3(pdppo)_2]$-PDMS	Eu^{III}	[A]	80–180	1.0	280	[*]
$[Tb(3,5\text{-}bbza)_3(pdppo)_2]$-PDMS	Tb^{III}	[A]	110–260	0.50	220	[*]
$[Yb(3,5\text{-}bbza)_3(pdppo)_2]$-PDMS	Yb^{III}	[A]	70–170	1.1	240	[*]
$YVO_4:Er^{III}$	CTB-Er^{III}	[A]	299-466	2.61	300	4
$[Eu(3,5\text{-}bbza)_3(pdppo)_2]$-PDMS	Eu^{III}	[B]	80–180	1.1	280	[*]
$[Tb(3,5\text{-}bbza)_3(pdppo)_2]$-PDMS	Tb^{III}	[B]	110–260	1.2	220	[*]
$[Yb(3,5\text{-}bbza)_3(pdppo)_2]$-PDMS	Yb^{III}	[B]	70–170	1.6	140	[*]
Ln-cpda (Ln = Eu, Tb)	Eu^{III}-Tb^{III}	[C]	40-300	16	300	5
pNdpal–EuTb	Eu^{III}-Tb^{III}	[C]	300-320	12.6	309	6
PDMS-eddpo-$Ln(bzac)_3$ (Ln = Eu,Tb)	Eu^{III}-Tb^{III}	[C]	158-248	11	203	7
$Tb_{0.01}Eu_{0.23}$-coordination polymers	Eu^{III}-Tb^{III}	[C]	294–373	10.67	373	8
$[(CH_3)_2NH_2]Eu_{0.036}Tb_{0.964}$BPTC	Eu^{III}-Tb^{III}	[C]	220-310	9.42	310	9
$[Ln(tfac)_3]\cdot 2H_2O$ (Ln = Eu, Tb)	Eu^{III}-Tb^{III}	[C]	293–343	7.1	293	10
$[Ln_2(L)_3\cdot NO_3]\cdot(NO_3)_2$ (Ln = Eu, Tb)	Eu^{III}-Tb^{III}	[C]	247-377	6.35	377	11
$[(Tb_{0.914}Eu_{0.086})_2(PDA)_3(H_2O)]\cdot 2H_2O$	Eu^{III}-Tb^{III}	[C]	10−325	5.96	25	12
$[Ln(btfa)_3(H_2O)_2]$ (Ln = Eu, Tb)	Eu^{III}-Tb^{III}	[C]	295–315	5.8	296	13
$Tb_{0.995}Eu_{0.005}$@In(OH)-bpydc	Eu^{III}-Tb^{III}	[C]	283-303	4.47	333	14
$Na_2K[(Lu_{0.75}Yb_{0.20}Er_{0.05})_3Si_6O_{18}$	Er^{III}-Yb^{III}	[C]	12-86	2.6	27	15
$Cs_2Ag_{0.6}Na_{0.4}InCl_6$:Bi,Yb	Bi^{I}-Yb^{III}	[C]	290-470	1.66	480	16
Ln-dpa (Ln = Eu, Tb)	Eu^{III}-Tb^{III}	[C]	293–333	1.5	293	17
LaF_3:Yb@ LaF_3:Nd	Nd^{III}-Yb^{III}	[C]	283-320	0.41	283	18
$LaLiP_4O_{12}$:Nd/Yb	Nd^{III}-Yb^{III}	[C]	100-600	0.4	330	19
$[Ln_2(NDC)_3(DMF)_2]$ Ln = Nd, Yb	Nd^{III}-Yb^{III}	[C]	20-300	0.2	300	20

[*] This work.

[A] Intensity ratio of two excitation bands. [B] Emission intensity ratio upon two-wavelength excitation. [C] Emission intensity ratio of two bands (dual center) upon the same excitation wavelength.

Abbreviations: btfa: 4,4,4-trifluoro-l-phenyl-1,3-butanedionate; dpa: di-(2-pyridyl)amide, tfac: 1,1,1-trifluoro-2,4-pentanedionate; bpydc: 4,4'-biphenyl-dicarboxylate; bzac: 1-phenyl-1,3-butanedione; PDMS: polydimethylsiloxane; cpda: 5-(4-carboxyphenyl)-2,6-pyridinedicarboxylate; H_2NDC: 2,6-naphthalenedicarboxylic acid. CTB = charge transfer band.

Supplementary references

[1] A. G. Bispo-Jr, I. O. Mazali, F. A. Sigoli, *Phys. Chem. Chem. Phys.,* 2022, Accepted Manuscript.

[2] R. D. L. Gaspar, S. M. M. Ferraz, P. C. Padovani, P. R. Fortes, I. O. Mazali, F. A. Sigoli, I. M. Raimundo Jr., *Sens. Actuators B Chem.*, 2019, **287**, 557.

[3] L. M. Johnson, L. Gao, C. W. Shields IV, M. Smith, K. Efimenko, K. Cushing, J. Genzer, G. P López, *J. Nanobiotechnology*, 2013, **11**, 22.

[4] I. E. Kolesnikov, D. V. Mamonova, M. A. Kurochkin, E. Yu. Kolesnikov, E. Lahderanta, J. Lumin., 2021, 231, 117828.

[5] Y. J. Cui, W. Zou, R. Song, J. Yu, W. Zhang, Y. Yang, G. Qian, *Chem. Commun.*, 2014, **50**, 719.

[6] J. Aparecida Sobrinho, G. A. Brito Junior, I. O. Mazali, F. A. Sigoli, *New J. Chem.*, 2020, **44**, 8068.

[7] D. A. Gálico, Í. O. Mazali, F. A. Sigoli, *J. Chem.*, 2018, **42**, 18541.

[8] J. K. Zareba, M. Nyk, J. Janczak, M. Samoć, *ACS Appl. Mater. Interfaces*, 2019, **11**,10435.

[9] Y. Pan, H-Q. Su, E-L. Zhou, H-Z. Yin, K-Z. Shaoc, Z-M. Su, *Dalton Trans.*, **2019**, 48, 3723.

[10] C. D. S. Brites, M. C. Fuertes, P. C. Angelomé, E. D. Martínez, P. P. Lima, G. J. A. A. Soler-Illia, L. D. Carlos, *Nano Lett.*, 2017,**17**, 4746.

[11] T. Zhou, S. Liu, S. Wang, S. Mi, P. Gao, X. Guo, Q. Su, H. Guo, *Ind. Eng. Chem. Res.*, 2021, **60**, 11760−11767.

[12] Z. Wang, D. Ananias, A. Carné-Sánchez, C. D. S. Brites, I. Imaz, D. Maspoch, J. Rocha, L. D. Carlos *Adv. Funct. Mater.*, 2015, **25**, 2824.

[13] R. Piñol, C. D. S. Brites, R. Bustamante, A. Martínez, N. J. O. Silva, J. L. Murillo, R. Cases, J. Carrey, C. Estepa, C. Sosa, F. Palacio, L. D. Carlos, A. Millán, *ACS Nano*, 2015, **9**, 3134.

[14] Y. Zhou, B. Yan, F. Lei, *Chem. Commun.,* 2014, **50**, 15235.

[15] D. Ananias, F. A. Almeida Paz, L. D. Carlos, J. Rocha, *Chem. Eur. J.*, 2018, **24**, 11926.

[16] S. Yang, S. Gong, Z. Zhou, L. Wu, M. Zhang, L. Jiang, W. Wu, B. Yb, *J. Phys. Chem. C*, 2021, **125**, 10431−10440.

[17] M. Rodrigues, R. Piñol, G. Antorrena, C. D. S. Brites, N. J. O. Silva, J. L.Murillo, R. Cases, I. Díez, F. Palacio, N. Torras, J. A. Plaza, L. Pérez-García, L. D. Carlos, A. Millán, *Adv. Funct. Mater.*, 2016, **26**, 200.

[18] E. C. Ximendes, W. Q. Santos, U. Rocha, U. K. Kagola, F. Sanz-Rodríguez, N. Fernandez, A. S. Gouveia-Neto, D. Bravo, A. M. Domingo, B. del Rosal, C. D. S. Brites, L. D. Carlos, D. Jaque, C. Jacinto, Nano Lett. 2016, **16**, 1695.

[19] Ł. Marciniak, A. Bednarkiewicz, M. Stefanski, R. Tomala, D. Hreniak, W. Strek, *Phys. Chem. Chem. Phys.,* 2015, **17**, 24315.

[20] G. E. Gomez, R. Marin, A. N. Carneiro Neto, A. M. P. Botas, J. Ovens, A. A. Kitos, M. C. Bernini, L. D. Carlos, G. J. A. A. Soler-Illia, M. Murugesu, *Chem. Mater.*, 2020, **32**, 7458.